Article

JOURNAL OF COMPOSITE MATERIALS

Journal of Composite Materials
0(0) 1–14

DOI: 10.1177/0021998317723967
journals.sagepub.com/home/jcm

SAGE

Structural and dielectric properties of hot-pressed poly(vinylidene fluoride)-based composites

E Ruggiero, MM Reboredo and MS Castro

Abstract

The characterization of ceramic/polymer composites was performed on zinc oxide/poly(vinylidene fluoride) – ZnO/PVDF and barium titanate/poly(vinylidene fluoride) composites with varying filler concentration in order to evaluate the main interactions responsible for the composite dielectric behavior. The materials, poly(vinylidene fluoride) and its composites, were melt-blended using a two-roller mixer and then hot-pressed. The permittivity of composites was enhanced compared with that of the pure poly(vinylidene fluoride) with the addition of 20 w/w% of ZnO particles. However, samples with 40 or 60 w/w% of ZnO registered a diminution in the real permittivity values which was connected to particle-matrix adhesion problems. On the other hand, barium titanate composites presented a more homogeneous morphology with less presence of voids and a better adhesion between the filler and the polymer, where real permittivity increased with the addition of barium titanate particles.

Keywords

Poly(vinylidene fluoride), polymer composite, $BaTiO_3$, ZnO, dielectric properties

Introduction

Dielectric composites containing a polymer matrix and ceramic particles have been widely studied due to the combination of the high dielectric performance of ceramics and the low cost and the easy processing of polymers. Such materials with high dielectric permittivity have opened opportunities for numerous applications, such as embedded capacitors, gate dielectrics, and electric energy storage devices.[1] Therefore, polymer–ceramic materials have aroused much attention for uses in microelectronics packaging.[2] It was also established that improvements in dielectric properties are linked to particles content, processing conditions and the matrix dielectric permittivity.[2] Certainly, polymer dielectric properties can be improved by ZnO or $BaTiO_3$ particles addition for integrated circuits.[3,4]

Zinc oxide (ZnO) is one of the most promising materials for optoelectronic, spintronic and piezoelectric devices due to its piezoelectric and optoelectronic properties.[5] Recently, it was reported that the incorporation of nanosized ZnO enhances the dielectric properties of PVDF piezoelectric polymer.[3,6] Moreover, Indra Devi et al. found that ZnO composition has a great influence on the trend and magnitude of dielectric properties, enhancing dielectric permittivity values.[6]

Barium titanate (BT) ceramic is a well-known ferroelectric ceramic that has been of practical importance because of its excellent dielectric properties. Especially, the tetragonal room temperature phase provides polarization from the titanium ion movement in c-dimension resulting in ferroelectric behavior.[7] Furthermore, tetragonal barium titanate is known for its high permittivity, its suitability for ac-currents of a wide frequency range.

Poly(vinylidene fluoride) (PVDF) has been widely investigated due to its outstanding pyro- and piezoelectric properties.[8] PVDF has been considered as an ideal polymer matrix for applications in micro-electronic devices, and high-charge storage capacitors due to its

Institute of Materials Science and Technology (INTEMA), University of Mar del Plata and National Research Council (CONICET), Argentina

Corresponding author:
MS Castro, Institute of Materials Science and Technology (INTEMA), University of Mar del Plata and National Research Council (CONICET), Av. Juan B. Justo 4302, Mar del Plata, Buenos Aires 7600, Argentina.
Email: mcastro@fi.mdp.edu.ar

high permittivity, and excellent properties.[9] Another essential characteristic of PVDF is polymorphism. Depending on their chain conformations as trans (T) or gauche (G) linkages, PVDF has five crystalline phases: non-polar α-phase and ε-phase, as well as polar β-phase, δ-phase, and γ-phase. However, α-and β-phase PVDF are the most investigated conformations.[10] α-phase is the most common crystal structure (TGTG), and can be formed during conventional melt and solution processing processes. β-phase has a trans planar zigzag structure (TTTT), which is responsible of the largest spontaneous polarization per unit cell compared with other crystal phases and contributes to the development of high pyro- and piezoelectric properties.[9,11]

There are two main objectives in the present research work. The first one aims to determine the influence of the way in which commercial PVDF is provided (pellet or powder) on final properties of PVDF-hot pressed samples. The second one is to investigate the influence of $BaTiO_3$ and ZnO particles addition into a PVDF matrix on the structure, microstructure and dielectric behavior. Composites were hot-pressed and the resulting properties were mainly evaluated by X-ray diffraction, Fourier transform infrared spectroscopy, scanning electron microscopy and dielectric measurements. The final properties were correlated with the particles amount, the particle–matrix interaction, and the stabilized PVDF configuration after processing. In this work, two main achievements were made. One is associated with the selection of the PVDF matrix, taking into account both processing conditions and final dielectric properties, while the other is related to the improvement of dielectric properties of PVDF-based composites through a simple processing route.

Materials and methods

Size particle distributions of the inorganic particles, ZnO (Baker Analyzed ACS Reagent, J.T.Baker®) or BT (Ferro Corporation Code 219-6) were determined by the Sedigraph technique with a Micromeritics. Two grades of PVDF were used in this work, PVDF powder (3M) and pellets (Dyneon PVDF 6008/0001 – 3M) supplied by 3M Argentina SACIFIA.

PVDF pellets or powders with or without particles were melt-blended at 200°C and 100 r/min for 10 min, using a two-roller mixer, Brabender type (own construction). The PVDF and PVDF/particles mixtures were inserted between two steel boards (diameter 2.5 cm × 1 mm) and molded by the hot-press method (Establecimiento Mario Smaniotto S.R.L, AMS 160/335 DF). In order to facilitate the composite preparation, weight fractions were used and the equivalent volume fractions are shown in Table 1.

Table 1. Weight and volume content.

Sample	Weight percentage	Volume percentage
PVDF/$BaTiO_3$	20	6.8
	40	16.4
	60	30.6
PVDF/ZnO	20	7.3
	40	17.4
	60	32.1

The hot-pressing process was performed at 16 MPa and 200°C for 15 min. The samples were cooled inside the press until 135°C and in air up to room temperature.

The thermal behavior was followed using a Shimadzu DSC-50 with a heating and cooling ramp of 10°C/min from room temperature to 200°C under nitrogen flow. The degree of crystallinity was measured as the ratio between ΔH_m and ΔH_0, where ΔH_m is the melting enthalpy of the material under study and ΔH_0 is the melting enthalpy of totally crystalline material ($\Delta H_0 = 104.50$ J/g for PVDF).[12] The Fourier transform infrared (FT-IR) analysis was performed on a Nicolet 6700, thermo Scientific Analyzer, from 400 to 2000 cm^{-1}. The X-ray diffraction (XRD) patterns of the samples were recorded by a Philips PW1830, using Cu(Kα) radiation (wavelength: 1.5405Å) at room temperature in the range of 2θ from 4 to 70° with a scanning rate of 1°/min.

Densities were measured using the Archimedes's method and theoretical composite density (ρ_C) was calculated using equation (1).

$$\rho_C = \varphi_f \rho_f + (1 - \varphi_f)\rho_m \quad (1)$$

where ρ_f is the filler density, ρ_m is the matrix density and φ_f is the volume fraction of filler.

For scanning electron microscopic (SEM) observation, samples were fractured under liquid nitrogen. Images were collected with a JEOL 6460LV.

Finally, for dielectric measurements, samples were painted with a silver paste and dielectric measurements were performed using a Hewlett Packard 4284A Impedance Analyzer from 20 Hz to 1 MHz.

Results and discussion

Characterization of fillers

Crystalline structure of ZnO and BT powders by XRD. Figure 1 presents the XRD pattern of ZnO and BT powder. All peaks of ZnO powders can be assigned to the hexagonal structure (*JCPDS 80-0075)* where

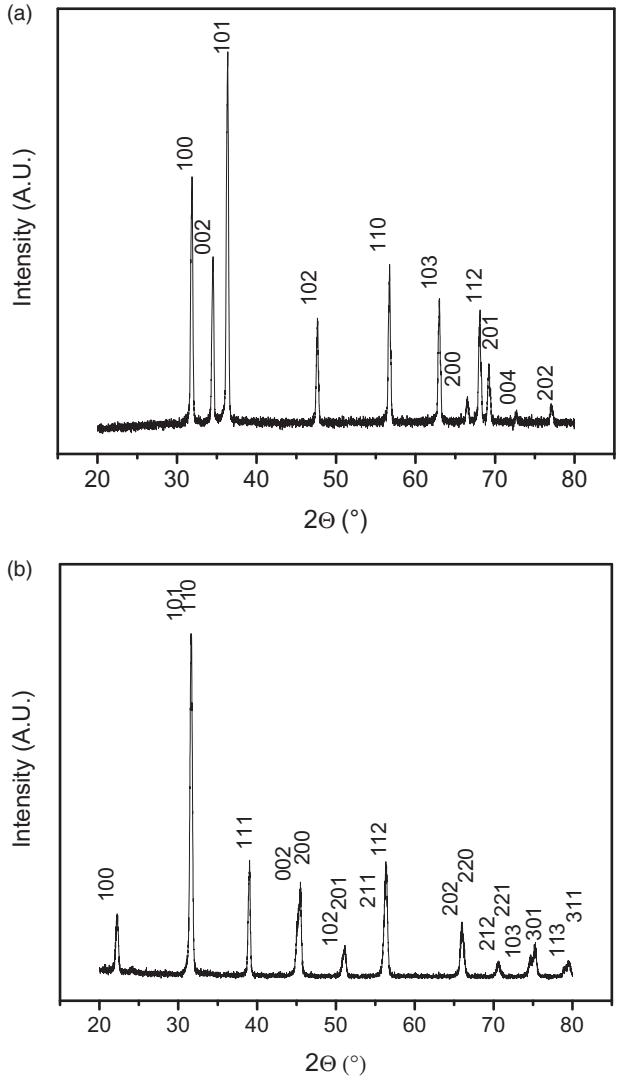

Figure 1. X-ray patterns of ZnO (a) and BT (b).

Table 2. Particle size distributions of ZnO and BT powders.

Sample	D_{10} (μm)	D_{50} (μm)	D_{90} (μm)	W
ZnO	0.27	2.7	7.8	2.79
BT	0.5	2.2	5.6	2.32

secondary phases are not observed (Figure 1(a)). Similarly, peaks in Figure 1(b) can be assigned to the tetragonal perovskite structure of BT (*JCPDS 83-1880*), without secondary phases.

Particle size and distribution. Table 2 shows data from the particle size distribution corresponding to ZnO and BT powders. D_{90}, D_{50} and D_{10} are the corresponding diameters of 90, 50 and 10% volume respectively, and $W = (D_{90}\text{-}D_{10})/D_{50}$ is a measure of the distribution width of particle size. Although medium particle of BT is close to that of ZnO, the particle size distribution of BT is narrower.

Figure 2(a) shows the morphology of ZnO powders where a mixture of spheroid-like and plate-like particles is observed. This morphological combination can be related with the broad particle size distribution observed. Figure 2(b) displays the scanning electron microcopy image of $BaTiO_3$ powders where a uniform spheroid-like morphology is observed.

PVDF samples from PVDF-pellets and PVDF-powders

Crystallization behavior of PVDF samples by DSC. DSC was used to characterize hot-pressed PVDF samples. It can be observed that samples from PVDF-pellet presented a higher and more defined melting point than samples from PVDF-powder (Figure 3(a)). Taking into account that the melting temperatures of α, β, and γ phases of PVDF are 165–170°C, 172–177°C, and 187–192°C, respectively, DSC results can be related with the higher β-PVDF amount in PVDF-pellet samples than in PVDF-powder samples.[12,13] Moreover, the crystalline degree of PVDF-pellet was close to 52.74% whereas it was 18.35% for PVDF-powder. Indeed, the crystallization temperature of PVDF-pellet is close to 139°C whereas for PVDF-powder it is 103°C (detected during the cooling program of the samples, see Figure 3(b)). Then, according to the opening mold conditions (135°C), samples from PVDF-powder are quickly cooled at room temperature decreasing its degree of crystallinity.

Crystalline structure of PVDF samples by XRD and FTIR. Figure 3(c) presents X-ray diffraction patterns of the PVDF-pellet and the PVDF-powder samples mixed and hot-pressed at 200°C. Secondary phases were not found in these samples. Moreover, only peaks corresponding to two polymorphic crystalline structures were detected (α-PVDF and β-PVDF, *JCPDS* 42-1650 and 42-1649[14,15]). As the simultaneous presence of α and β produces the overlap around $2\theta = 20°$, it is difficult to differentiate the existence of β phase in the plates. In addition, samples from PVDF-pellet presented a higher crystalline degree than samples obtained from PVDF-powder. These results are in concordance with the observed DSC thermograms.

In order to investigate the specific crystalline phase of different materials, FTIR was employed. Figure 3(d) shows FTIR spectra of hot-pressed samples obtained from PVDF-pellet and PVDF-powder. The identified regions are rich in information on the conformational isomerism of the chain, providing information on the α- and β-phase content. Bands at 615, 766, 795, 874, 974, 1070, 1148, 1182, 1210, 1383, 1402, 1432 and

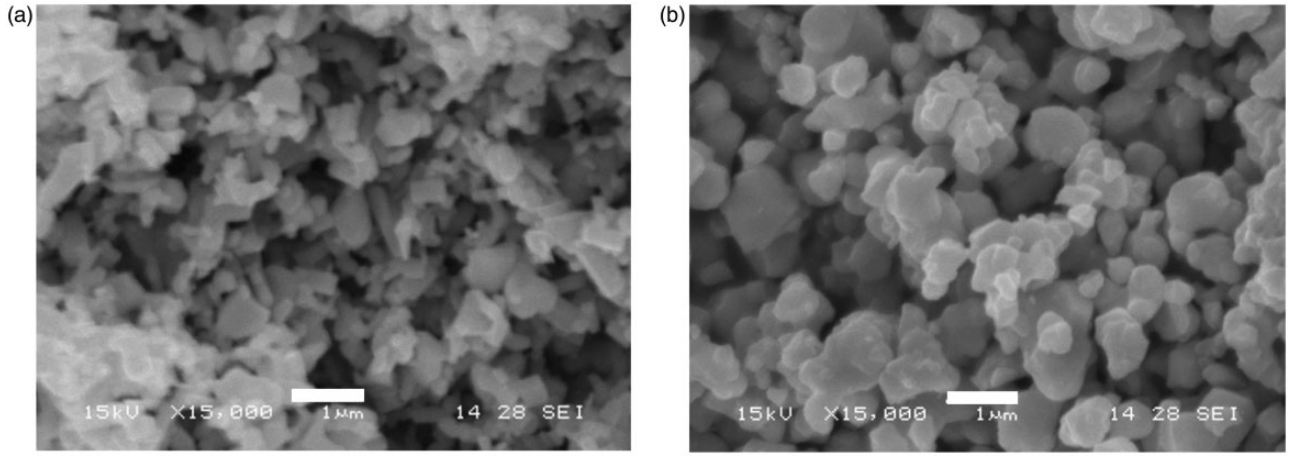

Figure 2. SEM images ZnO (a), and BT (b) powders. Bar = 1 μm.

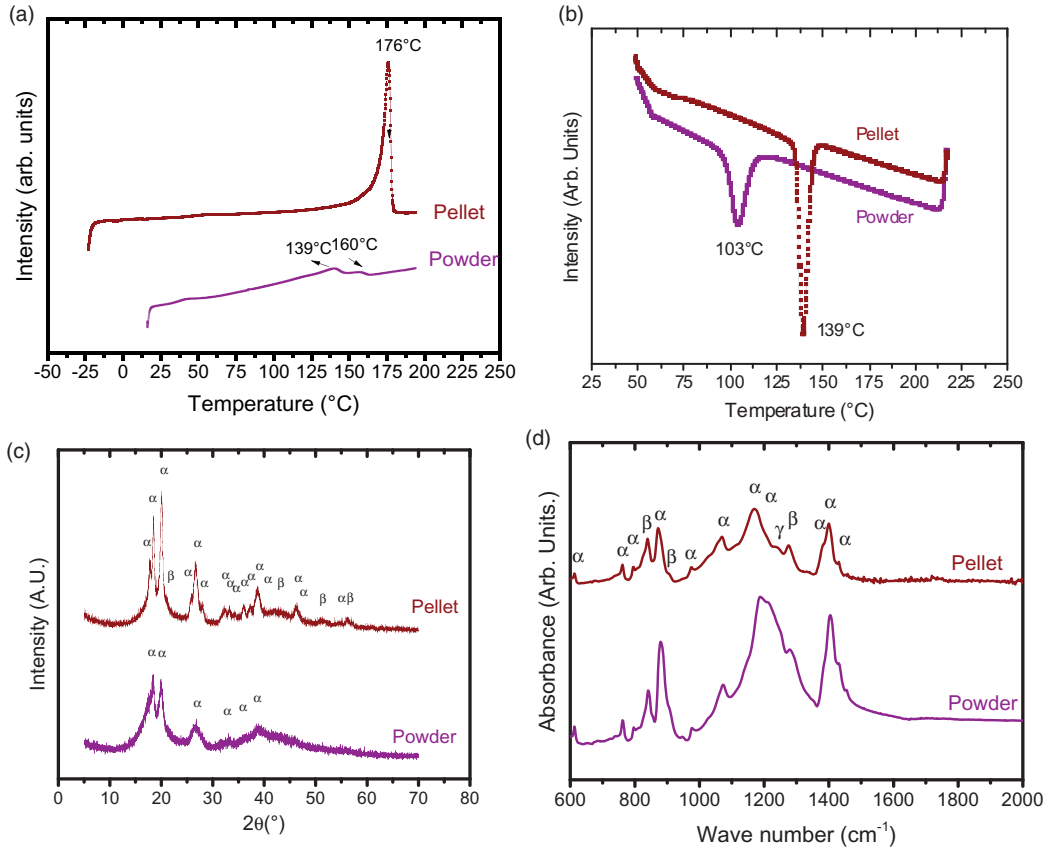

Figure 3. DSC thermograms during the heating (a) and the cooling (b) program, X-ray diffraction patterns (c), and FTIR spectra (d) of processed samples from PVDF-powder and PVDF-pellet.

1455 cm^{-1} can be associated to α-phase, whereas bands at 840, 882 and 1275 cm^{-1} are fingerprints of β-phase.[14,16–18] Interestingly, a small signal at 1235 cm^{-1} corresponding to γ-phase is also detected. From these results, it can be concluded that both samples majorly have the α-crystal phase and β-phase in a less degree.

PVDF samples morphology. Table 3 shows measured densities and the corresponding relative porosity of

samples made of PVDF-powder and PVDF-pellet. Samples processed from PVDF-pellet were more porous than PVDF-powder, at the processing temperature, due to the higher viscosity of PVDF-pellet which makes mixing difficult. Consequently, during the mixing process, air is retained inside the mixture, and after hot pressing, pores are generated in the composite.

Table 3. Measured density and relative porosity of samples from different PVDF Theoretical density 1.77 g/cm^3 (3M Technical data of PVDF, http://multimedia.3m.com/mws/media/232036O/fluoroplastic-pvdf-60512-0000-data-sheet.pdf).

Sample	Measured density (g/cm^3)	Relative porosity (%)
PVDF-Powder	1.77	0.0
PVDF-Pellet	1.64	7.34

Figure 4(a) and (b) presents microscopy images of fractured samples. Microstructure of samples processed from PVDF-powder shows a dense microstructure whereas in samples from PVDF-pellet small pores are observed. In addition, a ductile behavior was observed in all samples.

Dielectric performance of PVDF samples. Figure 4(c) and (d) shows the real permittivity and loss tangent curves of the PVDF processed samples. Samples obtained from PVDF-powder present higher real permittivity than samples from PVDF-pellet. This behavior can be related with the final porosity values. In addition, the low crystalline degree could influence the real permittivity values. Karasawa et al.[19] obtained real permittivities between 8 and 13 for the amorphous phase whereas values between 2 and 3 were registered for the crystalline phase. They found a localized soliton-like torsional defect that diffuses along the chain in

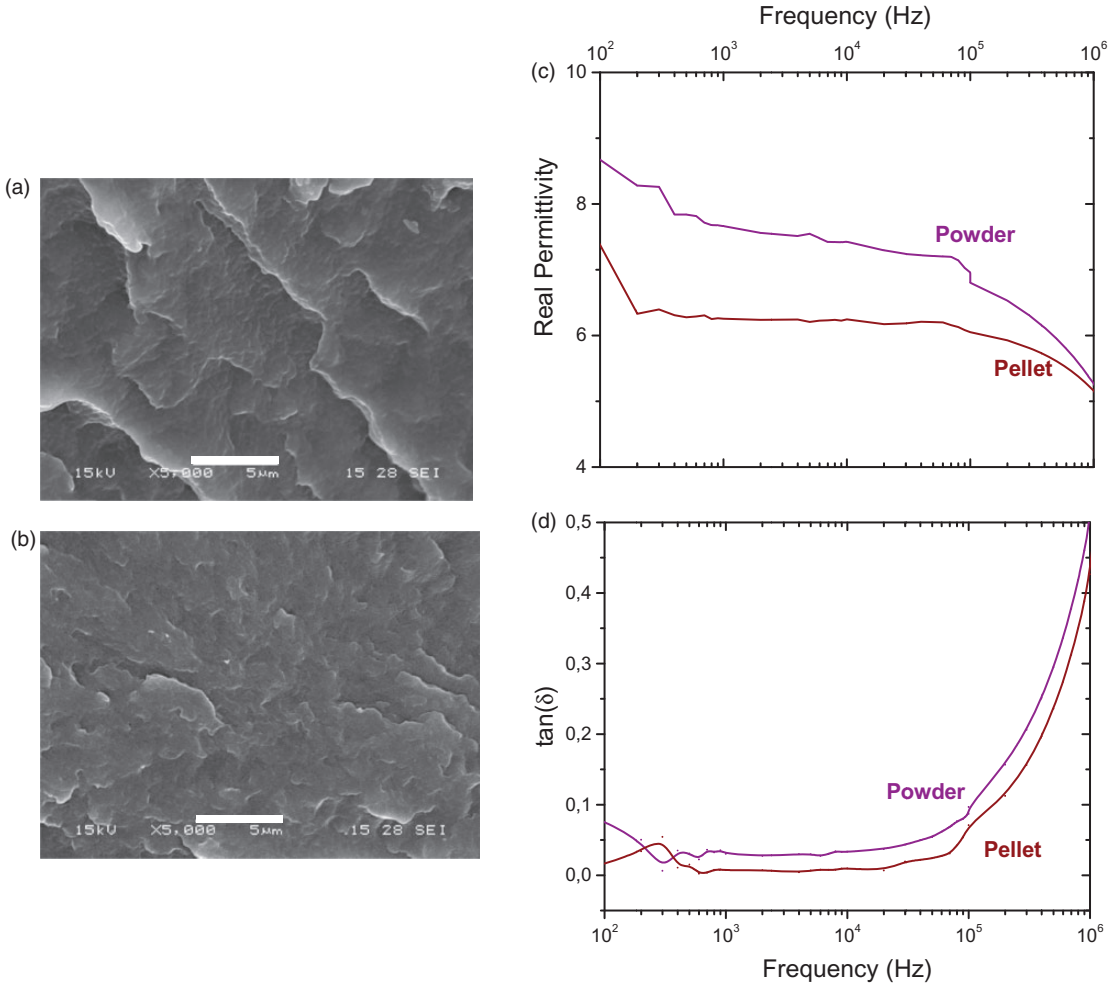

Figure 4. SEM images ((a) powder and (b) pellet) and Real Permittivity and loss tangent curves vs. frequency ((c) and (d)) of samples processed from PVDF-powder and PVDF-pellet.

the amorphous system provoking large dielectric constants. It is known that the β-phase is responsible for the superior ferroelectric and piezoelectric properties of PVDF films.[15] Taking into account that both samples present low β-phase/α-phase ratio, the low crystalline degree of PVDF-powder results in the major contribution to the permittivity values increasing. Moreover, polymers are materials of complex structure both at molecular and crystalline levels and the heterogeneity determines their properties. Dipolar segment parts of the main chain and side groups of various length scales can rotate resulting in a variety of relaxation processes appearing also in dielectric studies.[20] Consequently, it is difficult to ascribe a given dielectric relaxation to a molecular process in a polymer. The observed increasing in the loss tangent at the highest frequencies (10^6 Hz) can be assigned to molecular motions in the interior of the crystalline regions, with wide-angle oscillation of polar groups attached to main chain, followed by their rotation with the main chain cooperation,[21] and is due to the glass transition relaxation of PVDF. Moreover, the small dielectric permittivity and loss tangent rise at the lowest frequencies can be associated to molecular movements of large range at the PVDF crystalline region.

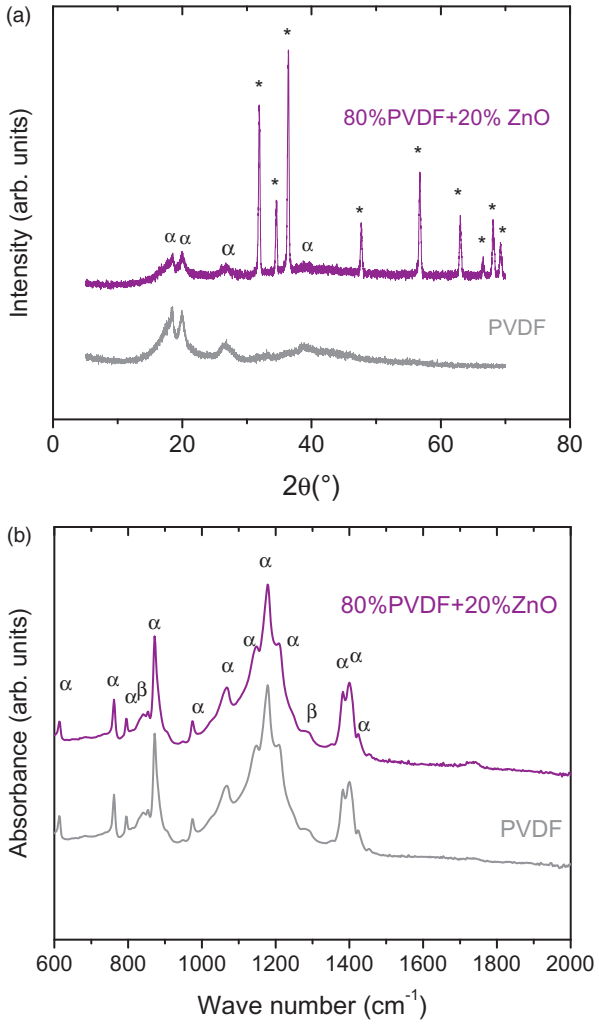

Figure 5. X-ray diffraction patterns (a) and FTIR spectra (b) of ZnO-PVDF composites.

According to the previous characterization, samples produced from PVDF-powder were selected for the composite processing because a denser microstructure and higher dielectric properties were achieved.

PVDF powder-ZnO composites

Structure of ZnO-PVDF composites by XRD and FTIR. Figure 5(a) shows the XRD pattern of ZnO-PVDF composites with 20w/w% filler addition. All peaks can be assigned to ZnO with hexagonal structure (*JCPDS 80-0075*) and α-PVDF (JCPDS42-1650). Peaks corresponding to β-PVDF cannot be assigned from this pattern.

In order to give a correct determination of the PVDF stabilized configuration, FTIR measurements were carried out. FTIR spectrum of hot-pressed ZnO-PVDF composites is presented in Figure 5(b). All signals can be attributed to α-PVDF and β-PVDF structures like in PVDF-powder samples. Through this spectrum, the apparition of β-phase in these composites is confirmed.

Crystallization behavior of ZnO-PVDF composites by DSC. Similar thermograms were obtained for all composites (not shown). From DSC thermograms, the crystallinity degrees were extracted (Table 4). Crystallinity values are a little higher when compared to those obtained for samples without the addition of ZnO particles. Yu et al. also observed that the incorporation of ceramic particles contributes to the increase of the crystallinity.[22]

The increase in crystallinity degree of samples can be attributed to particle–matrix interactions in the

Table 4. Crystallinity degree of ZnO- and BT-PVDF composites.

Sample	PVDF	20 ZnO + 80 PVDF	60 ZnO + 40 PVDF	20 $BaTiO_3$ + 80 PVDF	60 $BaTiO_3$ + 40 PVDF
Crystallinity (%)	18.35	21.5	23.2	20.2	19.25

composite. It is worth noting that the crystallization process is complex and influenced by several competing factors such as particle nature and content, presence of pores and processing conditions, among others.[23,24]

Composites morphology. Measured densities of composites are represented in Figure 6(a) and the corresponding theoretical values obtained from the rule mixture using the PVDF density (1.77 g/cm^3) and the ZnO density (5.606 g/cm^3). From the figure, it can be observed that experimental values are lower than theoretical ones.

SEM images of the composites with 20 and 60 w/w% of ZnO are shown in Figure 6(b) and (c), respectively, where adhesion problems between particles and matrix are detected due to the irregular geometric shapes of ZnO that contributes to making the dispersion process difficult. These adhesion troubles are responsible of the difference between the experimental and theoretical density values. Inset of Figure 6(c) shows an enlargement of the microstructure revealing the separation between particles and matrix.

Dielectric performance of ZnO-PVDF composites. Usually, the introduction of inorganic fillers into a polymer enhances the dielectric constant and loss values because the electrically conductive particles induce the extra charge carrier in the composite material. Consequently, when the ZnO filler level increases, the dielectric constant and loss values should raise. This can be explained by means of the interfacial space charge polarization. When the filler loading level is higher, the total effective area of the interfaces between the polymer matrix and the fillers are larger, which increases the interfacial space charge polarization.[6] Moreover, Bhunia et al. observed significantly larger values for dielectric constant when ZnO-PVDF composites were poled.[25] They attributed this behavior to the alignment of ZnO nanocrystals in the PVDF host matrix upon poling: the host PVDF matrix would render one of its surfaces to be fluorine-terminated while the other would be hydrogen-terminated resulting in alignment of the dipoles, producing a strong electric field within the host PVDF matrix. Consequently, the embedded ZnO crystals would also tend to orient themselves in their preferred c-axis orientation across the thickness of the PVDF film resulting in further enhancement of dipole moments in the composite films.[25]

Figure 7(a) and (b) presents real permittivity and loss tangent vs. frequency values of ZnO-PVDF

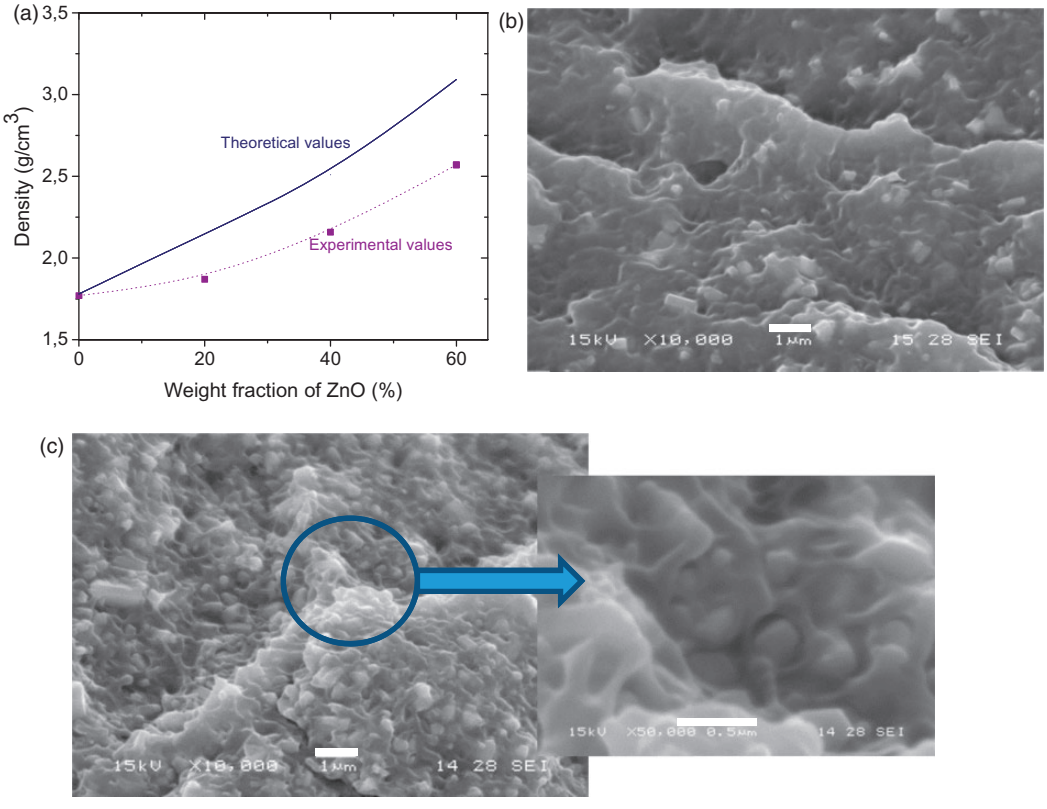

Figure 6. Theoretical and experimental density values of ZnO-PVDF composites (a), and SEM images of 20 w/w% ZnO-80 w/w% PVDF (b) and 60 w/w% ZnO-40 w/w% PVDF (c). Bar: 1 μm. The insert shows the enlargement of (c) (bar = 0.5 μm).

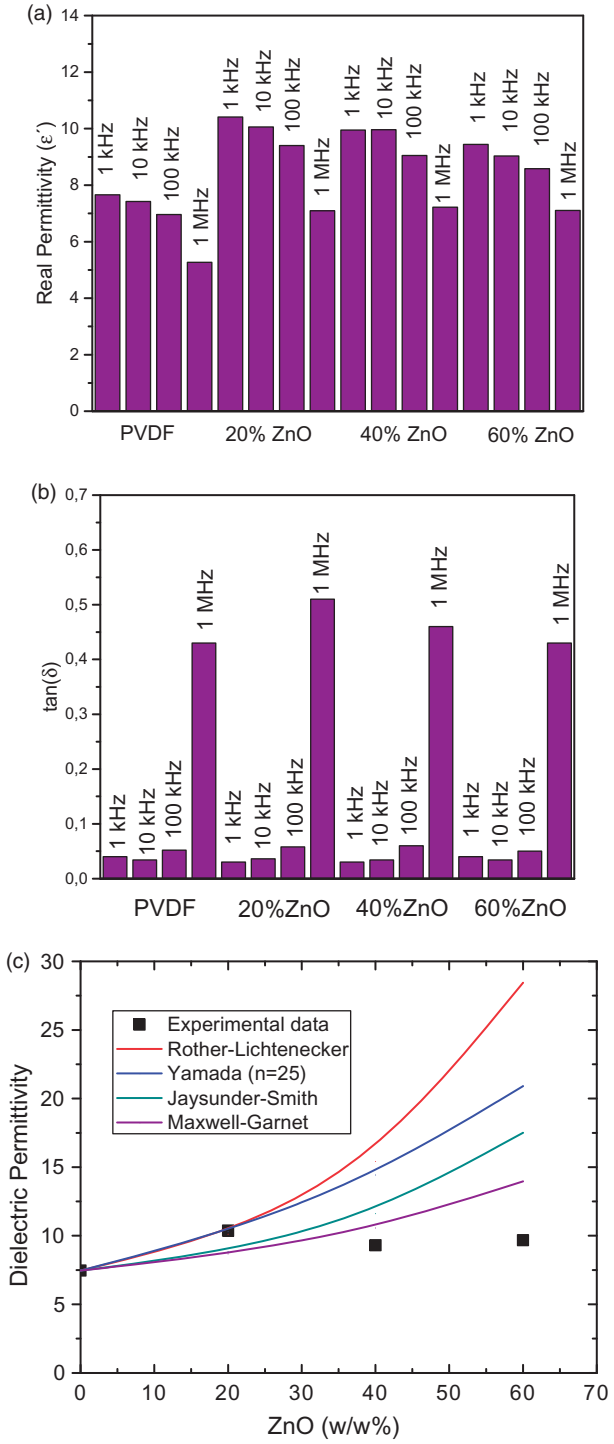

Figure 7. Real Permittivity and loss tangent values at different frequencies (a) and (b), and experimental and calculated real permittivity values at 1 kHz for ZnO-PVDF composites (c).

composites including pure PVDF values at room temperature. As generally expected, the permittivity of composites is enhanced compared with that of the pure PVDF with the addition of 20 w/w% of ZnO particles. However, samples with 40 or 60 w/w% of ZnO registered a diminution in the real permittivity values. Moreover, samples with 60w/w% ZnO registered the lowest real permittivity and the highest loss tangent values in all the studied frequencies. This reduction can be connected with the decrease in the composite density due to particle–matrix adhesion problems. Furthermore, considering that in order to improve composites properties, it is important to control the filler uniform dispersion in polymer matrix as well as the interaction of different components,[26] the reduction in the ZnO particles freedom orientation and main-chain flexibility of the PVDF matrix can also reduce dielectric properties. Specially, the presence of hexagonal disk-like ZnO particles could prevent the main-chain flexibility of polymer molecules.[26] The combination of all these factors contributes to decrease the dielectric properties for high ZnO particles additions.

Figure 7(c) presents real permittivity values calculated from the Maxwell-Garnet model (equation (2)) which considers the dielectric permittivity arising from spherical fillers dispersed in a medium and the Jaysundere-Smith (equation (3)) model which considers that at higher concentration of fillers, the interaction between fillers is becoming significant because the distance between fillers is extremely close, especially for nanosized fillers. Moreover, electrical field arising from the neat induced distribution of dipole moment is no more negligible when calculating overall field locally experienced in the matrix. Based on this assumption, Jaysundere and Smith proposed a more realistic mixing rule. They calculated the electric field with a dielectric sphere embedded in a continuous dielectric medium by taking into account polarization of adjacent particles[27]

$$\varepsilon'_{c=}\varepsilon'_m\left[1+\frac{3\varphi_f\left(\varepsilon'_f-\varepsilon'_m\right)}{\left(1-\varphi_f\right)\left(\varepsilon'_f-\varepsilon'_m\right)+3\varepsilon'_m}\right] \tag{2}$$

where ε'_c is the composite, ε'_f is filler, and ε'_m the matrix dielectric permittivity, and φ_f is the volume fraction of filler.

$$\varepsilon'_{c=}\frac{\varepsilon'_m\varphi_m+\varepsilon'_f\varphi_f\frac{3\varepsilon'_m}{\left(2\varepsilon'_m+\varepsilon'_f\right)}\left[1+3\varphi_f\frac{\left(\varepsilon'_f-\varepsilon'_m\right)}{2\varepsilon'_m+\varepsilon'_f}\right]}{\varphi_m+\varphi_f\frac{3\varepsilon'_m}{\left(2\varepsilon'_m+\varepsilon'_f\right)}\left[1+3\varphi_f\frac{\left(\varepsilon'_f-\varepsilon'_m\right)}{2\varepsilon'_m+\varepsilon'_f}\right]} \tag{3}$$

where φ_m is the volume fraction of matrix.

Rother–Lichtenecker's equation (equation (4)), for the dielectric function of a two-phase composite, is based on the Wiener theory for bounds of effective dielectric function or effective conductivity of a

composite,[28] where n is a shape parameter attributed to the shape of the particles.

$$\ln \varepsilon_c' = ln\varepsilon_m' + n.\varphi_f ln\left(\frac{\varepsilon_f'}{\varepsilon_m'}\right) \quad (4)$$

Yamada et al. derived an equation (equation (5)) for dielectric calculation of a binary system which is composed of a continuous medium of the dielectric constant and ellipsoidal particles[29]

$$\varepsilon_c' = \varepsilon_m'\left[1 + \frac{n\varphi_f(\varepsilon_f' - \varepsilon_m')}{n\varepsilon_m' + (1-\varphi_f)(\varepsilon_f' - \varepsilon_m')}\right] \quad (5)$$

where n is the morphology factor depending upon the shape of the particles and their orientation in relation to composite sample surface.

The dielectric constant of a material generally comprises four types of contributions, namely, electronic, ionic, orientational and space charge polarizations. Indeed, dielectric permittivity of ZnO bulk is close to 8.66,[30] while ZnO particles show values between 200 and 300 at 1 kHz.[31] The ZnO particles exhibit space charge polarization due to their structural inhomogeneities at the grain boundaries. These surface defects cause a change of positive and negative space charge distributions at the interfaces. When an external electric field is applied, these space charges move under the field and are trapped by defects at the interfaces, forming dipoles. At low frequencies, hopping electrons are trapped by these structural inhomogeneities which lead to a dominant space charge polarization at low frequencies. For a typical n-type semiconductor, the large amount of oxygen vacancies acts as shallow donors in ZnO. These oxygen vacancies appear at the interfaces of ZnO particles. Positive oxygen vacancies together with the negative oxygen ions produce a large amount of dipole moments. These dipole moments rotate in an external electric field, leading to rotational direction polarization at the interfaces of n-type ZnO particles. At higher frequencies, the space charges cannot follow the change of the field and hence do not produce space charge polarization. The dipoles are also unable to follow rapidly with varying electric field. Damping of these dipoles accounts for the reduction of dielectric constant at higher frequencies.[32–34] Consequently, dielectric permittivity of ZnO particles used for modeling at 1 kHz was 60 (higher than the corresponding for ZnO bulk) and 7.46 for PVDF. Experimental results deviate from theoretical models, most likely due to adhesion problems between particles and matrix and the presence of residual pores in the matrix. Furthermore, the formation of conducting paths for high particle volumes and different particles morphologies could influence the permittivity values. Indeed, fittings with different morphology factors were employed in the Yamada's model.

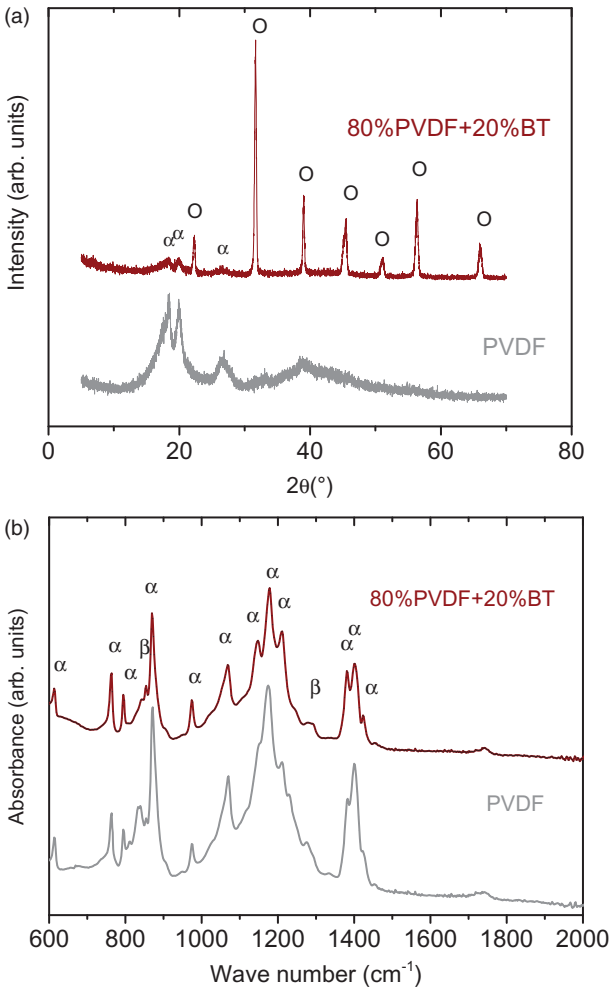

Figure 8. X-ray diffraction patterns (a) and FTIR spectra (b) of BT-PVDF composites.

BT-PVDF composites

Structure of BT-PVDF composites by XRD and FTIR. Figure 8(a) shows the XRD pattern of BT-PVDF composites with 20w/w% of filler addition. All diffraction peaks can be assigned to BT with tetragonal structure (*JCPDS 83-1880*) and α-PVDF (JCPDS42-1650). Peaks corresponding to β-PVDF cannot be assigned from this pattern.

FTIR spectrum of hot-pressed BT-PVDF composites is presented in Figure 8(b). All signals can be attributed to α-PVDF and β-PVDF structures like in PVDF-powder sample.

Crystallization behavior of BT-PVDF composites by DSC. Muralidhar et al. concluded that interactions

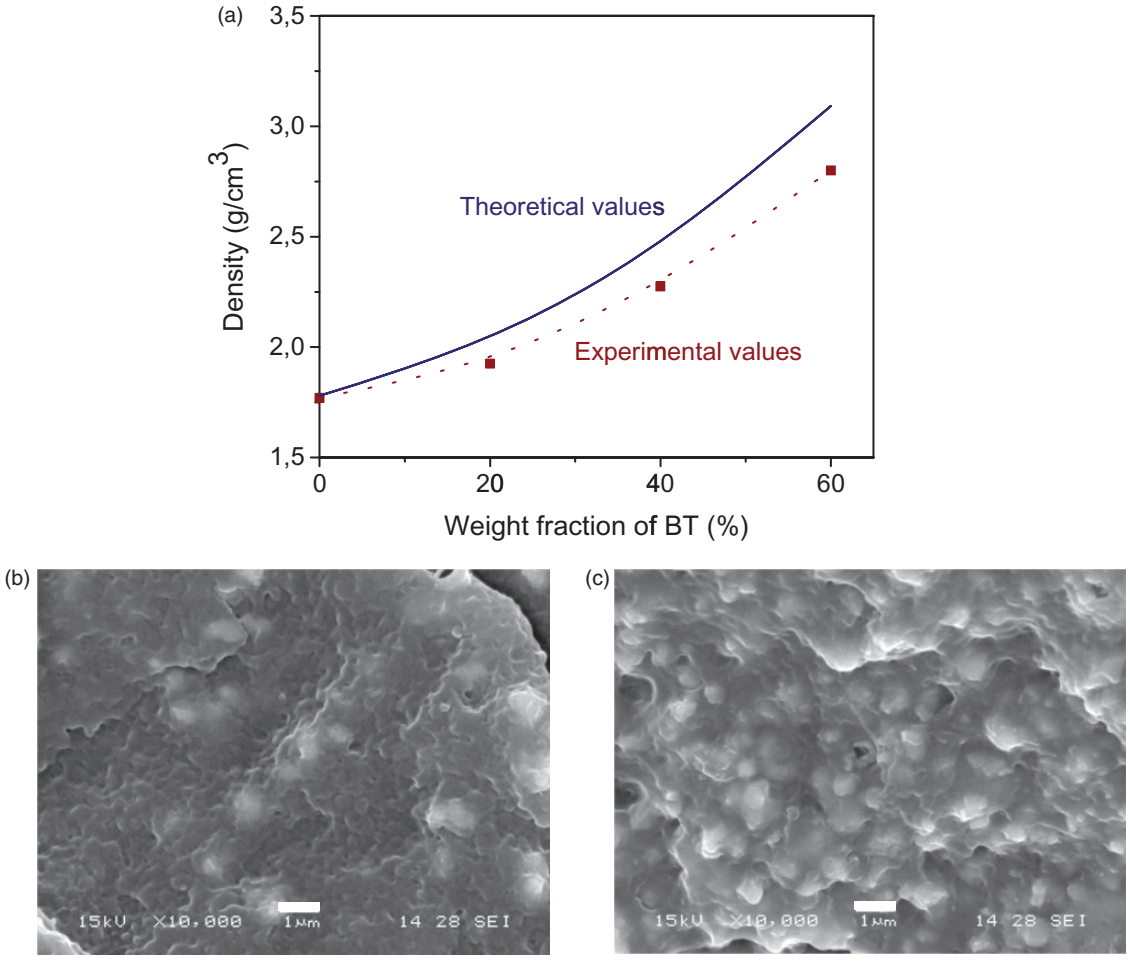

Figure 9. Theoretical and experimental density values of BT-PVDF composites (a), and SEM images of 20 w/w% BT-80 w/w% PVDF (b) and 60 w/w% BT-40 w/w% PVDF (c). Bar = 1 μm.

between PVDF and BT cannot be neglected because they found variations in the melting point and heat of fusion of PVDF in BT/PVDF composites as the weight fraction of BT is varied.[35] However, in this study, similar thermograms (not shown) were obtained for all composites. From DSC-thermograms the crystallinity degrees were extracted (see Table 4). Crystallinity values were close to that obtained for samples without the addition of $BaTiO_3$ particles, however lower than those with ZnO particles.

Composites morphology. Measured densities of composites are represented in Figure 9(a) and the corresponding theoretical values obtained from the rule mixture using the PVDF density (1.77 g/cm^3) and the BT density (6.02 g/cm^3). It can be observed that experimental values are lower than the theoretical ones but closer to them in comparison to ZnO composites.

SEM images of the composites with 20 and 60 w/w% of BT are shown in Figure 9(b) and (c). A good adhesion between particles and matrix is observed. Particles are completely embedded with the matrix and uniformly distributed through the composite. The observed voids can be attributed to residual pores in the composite or to particles removed from the fractured surfaces.

Dielectric performance of BT-PVDF composites. It is known that the size and crystalline phases of particles would influence the dielectric properties of the polymer composite films, but the concrete consequences on composites largely depends on the nature of the polymer matrix.[1] The relaxation processes in the polymer matrix determine the dielectric response of the composites but with higher permittivity values are attributed to the presence of BT.[36] Moreover, the conductivity and dielectric constant values of composites with nano BT filler are higher than those of the micron sized BT filler and the nanofiller fineness provides large surface area to the shielding material because of the presence of large number of active atoms at the material surface.[37]

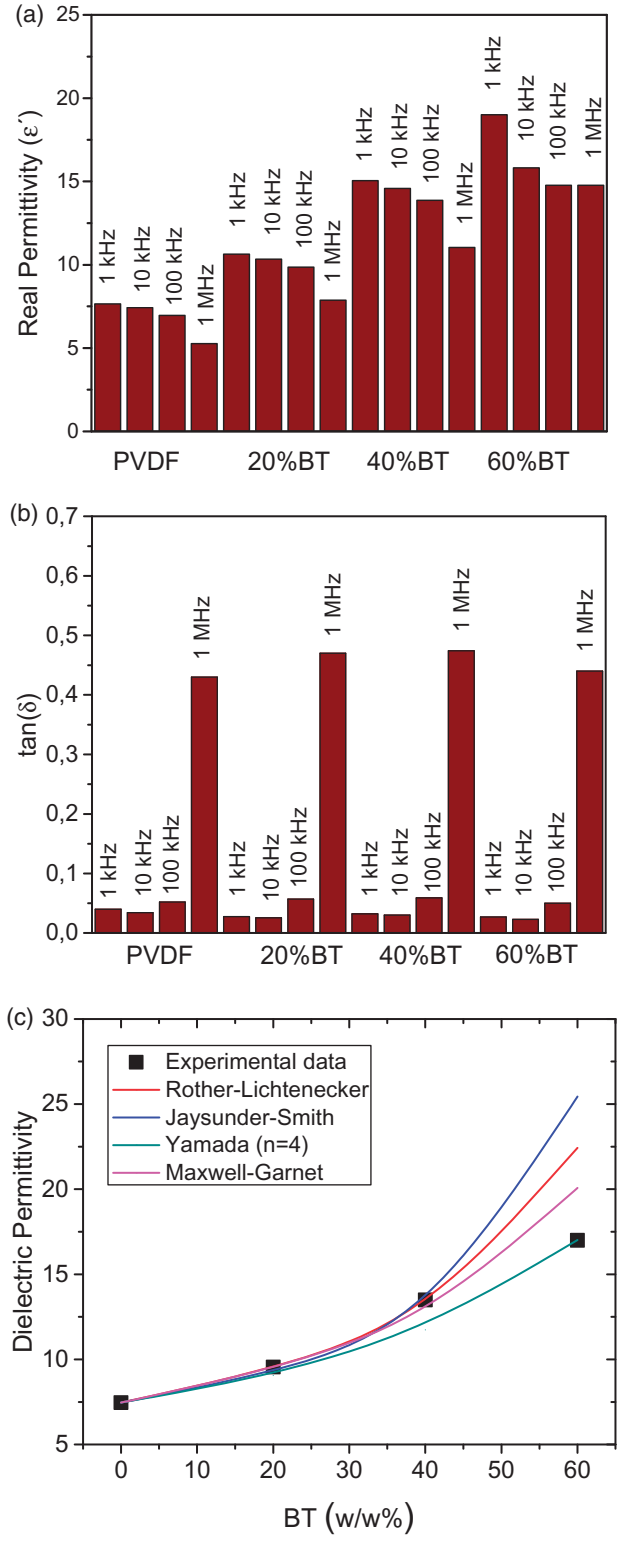

Figure 10. Real Permittivity and loss tangent values at different frequencies (a) and (b), and experimental and calculated real permittivity values (c) for BT-PVDF composites.

Table 5. Comparative results of dielectric permittivity at 1 kHz and porosity of ZnO and BT based PVDF composites.

Filler Amount	Real permittivity ZnO-PVDF	Relative porosity (%)	Real permittivity $BaTiO_3$-PVDF	Relative porosity (%)
0	7.66	0.56	7.66	0.56
20	10.41	13.02	10.64	6.1
40	9.95	14.02	15.05	8.27
60	9.44	16.88	19.01	9.44

Silakaew et al. found that different preparation methods have remarkable influences on the microstructure and dielectric properties of BT/PVDF nanocomposites.[38] Dielectric permittivity of BT/PVDF nanocomposites prepared by a liquid phase-assisted dispersion method was found to bring a homogeneous dispersion of BT nanoparticles in the PVDF matrix. Large clusters of agglomerated BT nanoparticles were observed in the BT/PVDF nanocomposite samples prepared by a solution processing method. That special microstructure resulted in the observed abnormally enhanced low-frequency dielectric permittivity behavior. That response can be attributed to the strong dipole polarization in the large clusters of agglomerated BT nanoparticles and high-intensity interfacial polarization at the large interface area of PVDF thin layer.[38]

Figure 10(a) and (b) presents real permittivity and loss tangent vs. frequency values of BT-PVDF composites. Real permittivity increases with the addition of BT particles whereas dielectric losses were not influenced by the filler amount. Figure 10(c) presents real permittivity values calculated from Maxwell–Garnet, Rother–Lichtnecker, Jaysundere–Smith and Yamada models using the BT and the PVDF real permittivity values (500 and 7.46, respectively). Experimental results showed the same trend than the calculated values. Differences between experimental and calculated values can be related to trapped pores with the highest filler amount. Moreover, considering that porosity problems are observed for the highest filler amount the Rocher–Lichtenecker's and Jaysunder–Smith's models do not adjust appropriately experimental results.

Dielectric constant of 31.4 were obtained with 60 wt% $BaTiO_3$ (85–128 nm) nanoparticles (31.5 vol%) addition to PVDF[39] while similar values were obtained with 30 vol% BT–PVDF film using a BT crystal size of 27.3 nm.[40] The low dielectric permittivity values obtained in this work can be associated to the filler particle size.

Table 5 resumes real permittivity and porosity values of ZnO- and BT-based PVDF composites. The higher real permittivity values obtained with BT filler addition than the ones with ZnO addition can be related to the

Table 6. Real permittivity (ε') of ZnO-PVDF and $BaTiO_3$-PVDF composites as reported in the literature.

Matrix	Crystallinity	Particle type	Particle size	Particle content (in volume)	ε'	Reference
PVDF	–	$BaTiO_3$	80–100 nm nearly spherical	0.3	40 @ 1 kHz	41
PVDF	Mostly α-phase	$BaTiO_3$	~100 nm	0.3	28 @ 1 kHz	22
PVDF	–	$BaTiO_3$	1 μm nearly spherical	0.3	31 @ 100 Hz	42
PVDF	–	$BaTiO_3$	50 nm	0.6	52 @ 1 kHz	43
			500 nm		70 @ 1 kHz	
PVDF	Mostly α-phase	$BaTiO_3$	2.2 μm	0.068	11 @ 1 kHz	This work
				0.306	20 @ 1 kHz	
PVDF	β-phase	ZnO	18 nm	0.034	10 @ 10 kHz	6
				0.073	11.6 @ 10 kHz	
				0.119	13 @ 10KHz	
PVDF	–	ZnO	~50 nm	0.032	11.9 @ 1 kHz	44
				0.059	12.7 @ 1 kHz	
				0.086	15.5 @ 1 kHz	
PVDF	Mostly α-phase	ZnO	2.7 μm	0.073	10.5 @ 1 kHz	This work
				0.321	9.5 @ 1 kHz	

better matrix–filler interaction, the lower porosity, the narrow particle size distribution with spherical morphology, and the high dielectric response of BT particles.

Table 6 displays real permittivity values of ZnO-PVDF and BT-PVDF composites reported in literature. For low ZnO content, real permittivity of ZnO-PVDF composites resulted similar to those found in this work even though the differences in particle size. However, for the highest ZnO content addition, problems between particle and matrix are responsible for the low observed values. On the other hand, BT-PVDF rendered low real permittivities in all the studied range of particle content. This result could be associated with the matrix characteristics, the high particle size, and the processing conditions.

Conclusions

The proper selection of PVDF materials, namely PVDF powder and pellets, has influence on the overall resulting properties. Certainly, samples produced from PVDF-powder exhibited denser microstructures and higher dielectric properties.

Ceramic-polymer composites from zinc oxide/poly (vinylidene fluoride) and barium titanate/poly(vinylidene fluoride) were obtained. The permittivity of composites was enhanced compared with that of the pure PVDF with the addition of 20 w/w% of ZnO particles. However, samples with 40 or 60 w/w% of ZnO registered a diminution in the real permittivity values. Although ZnO powders present a wider particle size distribution, which could improve particles accommodation in polymer composites, the low particle–matrix adhesion, the formation of conducting paths for high particle volumes, and different particles morphologies reduce the dielectric behavior of ZnO-PVDF composites.

On the other hand, $BaTiO_3$/PVDF composites presented a more homogeneous morphology with less presence of voids and a better adhesion between the filler and the polymer. In these composites, real permittivity increased with the addition of BT particles.

The higher dielectric permittivity values obtained with BT addition than the ones with ZnO addition can be related with the better matrix–filler interaction, the lower porosity, the narrow particle size distribution with spherical morphology and the high dielectric response of BT particles.

Due to the presence of voids and/or weak adhesion in ZnO/PVDF composites, none of the theoretical models used for the calculation of the real permittivity could adjust the experimental values. Nevertheless, there are two models (Maxwell-Garnet and Yamada) which performed well in fitting experimental values for the BT/PVDF composites.

Acknowledgements

The authors would like to thank Lic. Daniel O. Erasmo and 3M Argentina SACIFIA who kindly supplied the polymers for this work.

Declaration of Conflicting Interests

The author(s) declared no potential conflicts of interest with respect to the research, authorship, and/or publication of this article.

Funding

The author(s) disclosed receipt of the following financial support for the research, authorship, and/or publication of this article: This work was supported by Consejo Nacional de Investigaciones Científicas y Técnicas (CONICET) [grant no. PIP 112-200801-01851], Agencia Nacional de Promoción Científica y Tecnológica (ANPCyT) [grant no. PICT N°2010-1612] and Universidad Nacional de Mar del Plata (UNMdP) [grant no. 15G/330], Argentina.

References

1. Fan B, Zha J, Wang D, et al. Preparation and dielectric behaviors of thermoplastic and thermosetting polymer nanocomposite films containing BaTiO3 nanoparticles with different diameters. *Compos Sci Techno* 2013; 80: 66–72.
2. Ramajo L, Reboredo M and Castro M. Dielectric response and relaxation phenomena in composites of epoxy resin with BaTiO3 particles. *Compos Part A* 2005; 36: 1267–1274.
3. Nguyen V, Rouxel D, Vincent B, et al. Influence of cluster size and surface functionalization of ZnO nanoparticles on the morphology, thermomechanical and piezoelectric properties of P(VDF-TrFE) nanocomposite films. *Appl Surf Sci* 2013; 279: 204–211.
4. Ehrhardt C, Fettkenhauer C, Glenneberg J, et al. BaTiO3–P(VDF-HFP) nanocomposite dielectrics–Influence of surface modification and dispersion additives. *Mater Sci Eng B* 2013; 178: 881–888.
5. Wang ZL and Song J. Piezoelectric nanogenerators based on zinc oxide nanowire arrays. *Science* 2006; 32: 242–246.
6. Indra Devi P and Ramachandran K. Dielectric studies on hybridised PVDFZnO nanocomposite. *J Exp Nanosci* 2011; 6: 281–293.
7. Ota T, Takahshi J and Yamai L. Effect of microstructure on the dielectric properties of ceramics. *Key Eng Mater* 1992; 66–67: 185–246.
8. Furukawa T and Seo N. Electrostriction as the origin of piezoelectricity in ferroelectric polymers. *Jpn J Appl Phys* 1990; 29: 675–680.
9. Tao M-M, Liu F, Ma B-R, et al. Effect of solvent power on PVDF membrane polymorphism during phase inversion. *Desalination* 2013; 316: 137–145.
10. Lovinger AJ. Annealing of poly(vinylidene fluoride) and formation of a fifth phase. *Macromolecules* 1982; 15: 40–44.
11. Tang C-W, Li B, Sun L, et al. The effects of nanofillers, stretching and recrystallization on microstructure, phase transformation and dielectric properties in PVDF nanocomposites. *Eur Polym J* 2012; 48: 1062–1072.
12. Lanceros-Méndez S, Mano JF, Costa AM, et al. FTIR and DSC studies of mechanically deformed β-PVDF films. *Sci Phys* 2001; B40: 517–527.
13. Satapathy S, Gupta PK, Pawar S, et al. Crystallization of β-phase Poly (vinylidene fluoride) films using dimethyl sulfoxide (DMSO) solvent and at suitable annealing condition, https://arxiv.org/abs/0808.0419 (arXiv:0808.0419), (accessed 17 February 2017).
14. Sekar R, Tripathi AK and Pillai RKC. X-ray diffraction and dielectric studies of a BaTiO3:PVDF composite. *Mater Sci Eng B* 1989; 5: 33–36.
15. Tiwari V and Srivastava G. Effect of thermal processing conditions on the structure and dielectric properties of PVDF film. *J Polym Res* 2014; 21: 587–593.
16. Kobayashi M, Tashiro K and Tadokoro H. Molecular vibrations of three crystal forms of poly(vinylidene fluoride). *Macromolecules* 1975; 8: 158–171.
17. Bormashenko Y, Pogreb R, Stanevsky O, et al. Analysis method vibrational spectrum of PVDF and its interpretation. *Polym Test* 2004; 23: 791–796.
18. Yang H-C, We Q-Y, Liang H-Q, et al. Thermally induced phase separation of poly(vinylidene fluoride)/diluent systems: Optical microscope and infrared spectroscopy studies. *J Polym Sci Pol Phys* 2013; 51: 1438–1447.
19. Karasawa N and Goddard WA. Dielectric properties of poly(viny1idene fluoride) from molecular dynamics simulations. *Macromolecules* 1995; 28: 6765–6772.
20. Hilczer B, Kułek J, Markiewicz E, et al. Dielectric relaxation in ferroelectric PZT–PVDF nanocomposites. *J Non-Cryst Solids* 2002; 305: 167–173.
21. Kułek J, Pawlaczyk C and Markiewicz E. Influence of poling and ageing on high-frequency dielectric and piezoelectric response of PVDF-type polymer foils. *J Electrost* 2002; 56: 135–141.
22. Yu K, Wang H, Zhou Y, et al. Enhanced dielectric properties of BaTiO3/poly (vinylidene fluoride) nanocomposites for energy storage applications. *J Appl Phys* 2013; 113: 034105.
23. Paul DR and Robeson PLM. Polymer nanotechnology: Nanocomposites. *Polymer* 2008; 49: 3187–3204.
24. Shin KY, Lee JS and Jang J. Highly sensitive, wearable and wireless pressure sensor using free-standing ZnO nanoneedle/PVDF hybrid thin film for heart rate monitoring. *Nano Energy* 2016; 22: 95–104.
25. Bhunia R, Ghosh D, Ghosh B, et al. Free-standing flexible nanocrystalline-ZnO-impregnated polyvinylidene fluoride composite thin films. *J Compos Mater* 2015; 49: 3089–3101.
26. Vural S, Köytepe S, Seçkin T, et al. Synthesis, characterization, UV and dielectric properties of hexagonal disk-like ZnO particles embedded in polyimides. *Mater Res Bull* 2011; 46: 1679–1685.
27. Dang Z-M, Yuan J-K, Zha J-W, et al. Fundamentals, processes and applications of high-permittivity polymer-matrix composites. *Prog Mater Sci* 2012; 57: 660–723.
28. Goncharenko AV, Lozovski VZ and Venger EF. Lichtenecker's equation: applicability and limitations. *Opt Commun* 2000; 174: 19–32.
29. Yamada T, Ueda T and Kitayama T. Piezoelectricity of a high-content lead zirconate titanate/polymer composite. *J Appl Phys* 1982; 53: 4328–4332.

30. Yang Y, Guo W, Wang X, et al. Size dependence of dielectric constant in a single pencil-like ZnO nanowire. *Nano Lett* 2012; 12: 1919−1922.
31. Sinha N, Ray G, Bhandari S, et al. Synthesis and enhanced properties of cerium doped ZnO nanorods. *Ceram Int* 2014; 40: 12337–12342.
32. Zamiri R, Singh BK, Dutta D, et al. Electrical properties of Ag-doped ZnO nano-plates synthesized via wet chemical precipitation method. *Ceram Int* 2014; 40: 4471–4477.
33. Lanje AS, Sharma SJ, Ningthoujam RS, et al. Low temperature dielectric studies of zinc oxide (ZnO) nanoparticles prepared by precipitation method. *Adv Powder Technol* 2013; 24: 331–335.
34. Soosen Samuel M, Koshy J, Chandran A, et al. Dielectric behavior and transport properties of ZnO nanorods. *Physica B* 2011; 406: 3023–3029.
35. Muralidhar C and Pillai PKC. Effect on the melting point and heat of fusion of PVDF in barium titanate (BaTiO3)/polyvinylidene fluoride (PVDF) composites. *Mater Res Bull* 1988; 23: 323–326.
36. Kułek J, Szafraniak I, Hilczer B, et al. Dielectric and pyroelectric response of PVDF loaded with BaTiO3 obtained by mechanosynthesis. *J Non-Cryst Solids* 2007; 353: 4448–4452.
37. Joseph N, Singh SK, Sirugudu RK, et al. Effect of silver incorporation into PVDF-barium titanate composites for EMI shielding applications. *Mater Res Bull* 2013; 48: 1681–1687.
38. Silakaew K, Saijingwong W, Meeporn K, et al. Effects of processing methods on dielectric properties of BaTiO3/poly(vinylidene fluoride) nanocomposites. *Microelectron Eng* 2015; 146: 1–5.
39. Li YC, Tjong SC and Li RKY. Dielectric properties of binary polyvinylidene fluoride/barium titanate nanocomposites and their nanographite doped hybrids. *Express Polym Lett* 2011; 5: 526–534.
40. Kobayashi Y, Tanase T, Tabata T, et al. Fabrication and dielectric properties of the BaTiO3polymer nano-composite thin films. *J Eur Ceram Soc* 2008; 28: 117–122.
41. Silakaew K, Saijingwong W, Meeporn K, et al. Effects of processing methods on dielectric properties of BaTiO3/poly(vinylidene fluoride) nanocomposites. *Microelectron Eng* 2015; 146: 1–116.
42. Dang Z-M, Shen Y and Nan C-W. Dielectric behavior of three-phase percolative NiBaTiO3/polyvinylidene fluoride composites. *Appl Phys Lett* 2002; 81: 4814.
43. Mao YP, Mao SY, Ye Z-G, et al. Size-dependences of the dielectric and ferroelectric properties of BaTiO3/polyvinylidene fluoride nanocomposites. *J Appl Phys* 2010; 108: 014102.
44. Chilvery AK, Batra AK and Thomas M. Investigation on characteristics of PVDF/ZnO nanocomposite films for high-k capacitors. *Phys Sci Int J* 2014; 4: 734–741.